



Room-light-induced indoor air purification using an efficient Pt/N-TiO₂ photocatalyst

Hongqi Sun, Ruh Ullah, Siewhui Chong, Hua Ming Ang, Moses O. Tadé, Shaobin Wang*

Department of Chemical Engineering and CRC for Contamination Assessment and Remediation of the Environment (CRC-CARE), Curtin University, GPO Box U1987, Perth, WA 6845, Australia

ARTICLE INFO

Article history:

Received 13 June 2011

Received in revised form 10 August 2011

Accepted 12 August 2011

Available online 19 August 2011

Keywords:

Visible light photocatalysis

Pt/N-TiO₂

VOCs

Indoor air quality

Gas-phase

ABSTRACT

A conceptual air purifier harvesting fluorescent room lights was tested in this study. Visible photocatalysis was applied to facilitate the degradation of volatile organic compounds (VOCs) on a highly efficient visible light photocatalyst, Pt/N-TiO₂ synthesised via a sol–gel process. The as-prepared photocatalyst was characterised by many techniques, such as XRD, XPS, UV–vis DRS, N₂ adsorption and SEM, etc. XPS spectra revealed that platinum was at a chemical state of 2+, while nitrogen existed as NO_x species. The unique chemical compositions made the photocatalyst respond to visible light with a band gap of 2.69 eV, and present a broad absorption shoulder extended further into infrared region. The photocatalytic activities under irradiations of $\lambda > 387$, 430 and 490 nm were evaluated by photodegradation of phenol solutions. Under UV–vis light, the Pt/N-TiO₂ exhibited 5.5 times higher activity than Degussa P25. Various gaseous pollutants were degraded by employing the Pt/N-TiO₂ in a batch reactor. The capability of photodegradation of VOCs under room lights was also proven by the decomposition of gaseous toluene in a continuous reactor using fluorescent lamps (6 × 10 W). The mechanism of the enhanced activity in degradation of VOCs and potential application were discussed.

© 2011 Elsevier B.V. All rights reserved.

1. Introduction

Indoor air quality (IAQ) has become a critical community concern due to increased personal time (over 80%) spent in indoor environment, such as home, office, car and shopping center. Unfortunately, IAQ was suggested to be even worse than outdoor environment, attributing to the continuously emitting sources of combustion by-products, cooking, construction materials, office equipment, and consumer products. The detected pollutants from such sources mainly include nitrogen oxides (NO_x), carbon oxides (CO and CO₂), particulates, and volatile organic compounds (VOCs) [1]. Many VOCs are known to be toxic and considered as carcinogenic, mutagenic, or teratogenic. Long-term exposure to VOCs leads to sick building syndrome (SBS), such as dizziness, dry or itchy skin, eye, nose and throat irritation, a dry cough, fatigue, headache, or asthma attack [2].

To improve IAQ, three strategies, e.g. source control, increased ventilation, and air cleaning have been suggested to remove VOCs in indoor environment. Source control is often ungovernable and avoidable in metropolis and increased ventilation just transfers pollutants from indoor to outdoor environment. For air cleaning, advanced oxidation processes (AOPs) have shown their superiority

over conventional adsorption, as they can completely destroy VOCs to H₂O and CO₂ [3], other than phase transfer from gas to solid [4]. Thermal oxidation destruction had been extensively studied and was generally operated at a higher temperature of 200–1200 °C, hence being cost intensive [5]. Moreover, thermally catalytic oxidation is not economically feasible at low pollutant concentrations, which is typical in indoor air.

Photodegradation has been proposed as a promising approach since it not only completely oxidises VOCs, but also occurs at room temperature and ambient pressure [6,7]. Due to high activity, long-term stability, non-toxicity and low cost, TiO₂ has been employed as a typical semiconductor-based photocatalyst [6,8–11]. In photocatalysis, a photocatalyst is activated by the photons with greater energy than the band gap, producing electron/hole pairs to carry out redox reactions [12]. The band gap of anatase TiO₂ is 3.2 eV, which requires the wavelength of light shorter than 387.5 nm, in ultraviolet (UV) region. It is known that UV exposure is severely dangerous, even more harmful to humans than VOCs in indoor. The photodegradation of VOCs under visible light therefore becomes highly desirable for the viable application, i.e. air purifier using visible light photocatalysis.

The key issue in the photocatalytic removal of VOCs under visible light lies in the extension of the absorption threshold of TiO₂. Previous studies suggested that nitrogen doping was an effective method to make TiO₂ respond to visible light region, and nitrogen doped TiO₂ was generally applied to degrade aqueous

* Corresponding author. Tel.: +61 8 9266 3776; fax: +61 8 9266 2681.

E-mail address: shaobin.wang@curtin.edu.au (S. Wang).

pollutants [13–15]. Recently, N-TiO₂ has been employed to decompose VOCs for indoor air purification [10,16]. However, the visible light extension was weak and the activity was rather low. In gas-phase reaction, deactivation of a photocatalyst by intermediates or carbonisation was another concern. Co-doping of a metal with nitrogen into TiO₂ has been proposed to both extend the absorption and enhance the photocatalytic stability under visible light irradiations. Higashimoto et al. [17] reported that photocatalytic activity of N-TiO₂ would be significantly increased by surface modification with vanadium species in the decomposition of VOCs and that the interaction of oxidation states between +IV and +V on N-TiO₂ surface played the key role in the enhancement. Nitrogen and nickel co-doped TiO₂ was prepared by Zhang and Liu [18], who reported that Ni₂O₃ was dispersed on the surface of TiO₂ to suppress the recombination of photo-induced electron/hole pairs. Apart from lanthanoid and transition metals, noble metals such as silver, palladium and platinum have shown much effectiveness in improving the activity of N-TiO₂ [19–21]. In the degradation of VOCs, Li et al. [22] reported that an increased quantum efficiency of photodegradation of VOCs was observed over Pt/TiO_{2-x}N_x. The enhancement was attributed to the better separation efficiency of photogenerated electron/hole pairs, higher interface electron transfer rate, and an increased number of surface hydroxyl radicals.

In previous studies, a mercury lamp has been generally selected as UV source, and xenon (or metal halide) lamp as visible light source. Few investigations have been reported using room light. To further explore the advantage of visible light photocatalysis being operated at room temperature and atmospheric pressure, ambient room lights (fluorescent lamps) were employed to photodegrade VOCs in this work. This investigation would underpin an ideal design of harvesting room lights for simultaneous indoor air purification.

2. Experimental

2.1. Materials

Titanium (IV) isopropoxide (TTIP) was used as a Ti-precursor and supplied by Aldrich Chemicals with a purity of 97%. Urea was applied as a nitrogen source, supplied by Ajax Finechem with a grade of 99%. Hexachloroplatinic acid (99.9%) was used as a Pt precursor and purchased from Sigma–Aldrich. The VOC gases were prepared by evaporation of liquid acetone, ethanol, trichloroethene (TCE), 2-propanol, *n*-hexane, and toluene received for Chem Supply with a purity of 99.5%. A reference material of TiO₂-P25 was received from Degussa, Germany. A cylinder of toluene at 100 ppm in air was supplied by BOC.

2.2. Preparation of photocatalysts

Pt/N-TiO₂ was prepared by a modified sol–gel process with acid assistance. 100 mL of ethanol, 20 mL of acetic acid and 20 mL of TTIP were mixed to produce *solution A*. 1 L of deionised water, 1 mL of HNO₃ (69.5%), 0.3250 g of H₂PtCl₆·6H₂O, 15.5474 g of urea and 20 mL of acetic acid were mixed as *solution B*. In an ice bath, *solution A* was added dropwise into *solution B* to carry out a controlled hydrolysis and then aged for 48 h. After evaporation at 80 °C, the dried gels were annealed in air at 400 °C for 4 h. Then a Pt(1.0 at. %)/N-TiO₂ photocatalyst was obtained. Degussa P25 (TiO₂, 75% anatase and 25% rutile, 20 nm, and $S_{\text{BET}} = 50 \text{ m}^2/\text{g}$) was used as a reference sample for a comparison.

2.3. Characterisation of photocatalysts

UV–vis diffuse reflectance spectra (DRS) of samples were recorded on a JASCO V 670 spectrophotometer with an \varnothing 60 mm

integrating sphere, and BaSO₄ as a reference material. The crystalline structure of samples was analysed by powder X-ray diffraction (XRD) using a Bruker D8-Advance X-Ray diffractometer with Cu K α radiation ($\lambda = 1.5418 \text{ \AA}$). Scanning electron microscopy (SEM), performed on a Zeiss Neon 40EsB FIBSEM, was used to evaluate the morphology, size and texture information of the samples. The Brunauer–Emmett–Teller (BET) surface area and pore size distribution were evaluated by nitrogen sorption at -196°C using a Quantachrome Autosorb AS-1. Chemical compositions of Pt (1.0 at. %)/N-TiO₂ were analysed by X-ray photoelectron spectroscopy (XPS) using Thermo Escalab 250 with a monochromatic Al K α X-ray source. All binding energies were calibrated by the C 1s peak at 284.6 eV arising from adventitious carbon [23].

2.4. Tests of photocatalytic activity

The photocatalytic activity of Pt/N-TiO₂ dependent on the wavelengths was evaluated by degradation of 25 ppm aqueous phenol solutions using a MSR 572/2 metal halide lamp (575 W, Philips) with various cut-off filters. The concentration of phenol solutions was monitored by a high performance liquid chromatograph (HPLC) using a C-18 column, and a UV detector set at $\lambda = 270 \text{ nm}$.

2.5. Photocatalytic decomposition of VOCs

Two reactors (batch and continuous) were applied to evaluate the performance of Pt/N-TiO₂ in decomposition of various VOCs, such as acetone, ethanol, TCE, 2-propanol, *n*-hexane, and toluene. A 1.2 L stainless steel reactor was employed to carry out the batch tests. Fig. 1(A) schematically shows the batch reactor and associated system. The irradiations were provided by a Newport Oriel Universal Xenon arc lamp (300 W), and were filtered by a cut-off filter to block the lights with wavelengths shorter than 387 nm ($\text{UVA} < 0.05 \text{ W/m}^2$). The photocatalyst (0.1 g) was immobilised on a Petri dish ($D = 7 \text{ cm}$), which was fixed by a stainless steel support. In a typical run, the catalyst was loaded into the reactor, which was flushed by an instrument-grade air for 2 h to maintain the humidity constant in each run. Then a certain amount of liquid acetone was injected into the reactor, at a level of ca. 200 ppm in control condition (without a catalyst). The mixed gas was then recycled by a dual syringe pump (Hamilton Microlab 500) and monitored by a GC–MS (Varian 3800/2200) until the concentration was stable. Then the light was switched on and the concentrations at varying reaction time were recorded by the GC–MS.

Fig. 1(B) shows the continuous reaction system using room lights from fluorescent lamps ($6 \times 10 \text{ W}$) as light sources. A cylinder was used to provide VOC flow (100 ppm toluene in air), and the flow rate was controlled by a mass flow controller at 65 mL/min. The toluene gas was flowing into the continuous reactor with three channels. At the bottom of each channel a stainless steel plate ($29 \times 20 \text{ cm}$) coated with 0.2 g of photocatalyst was fixed. The lights irradiated the photocatalyst through a Soda glass window. The energy distribution of the fluorescent lamp is centred at ca. 570 nm in the region from 390 to 670 nm. The transparent performance of Soda glass was tested to be higher than 95%. The concentration of toluene was analysed by a GC (SHIMADZU 2010) with a FID detector.

3. Results and discussion

3.1. XPS studies

N (1s) and Pt (4f) XPS spectra of Pt/N-TiO₂ are shown in Fig. 2(A and B). A weak peak at 399.8 eV was fitted in N (1s) spectrum and no signal peak was found at ca. 396 eV. According to previous investigations [13,15], the peaks at the range of 399–401.5 eV arise from

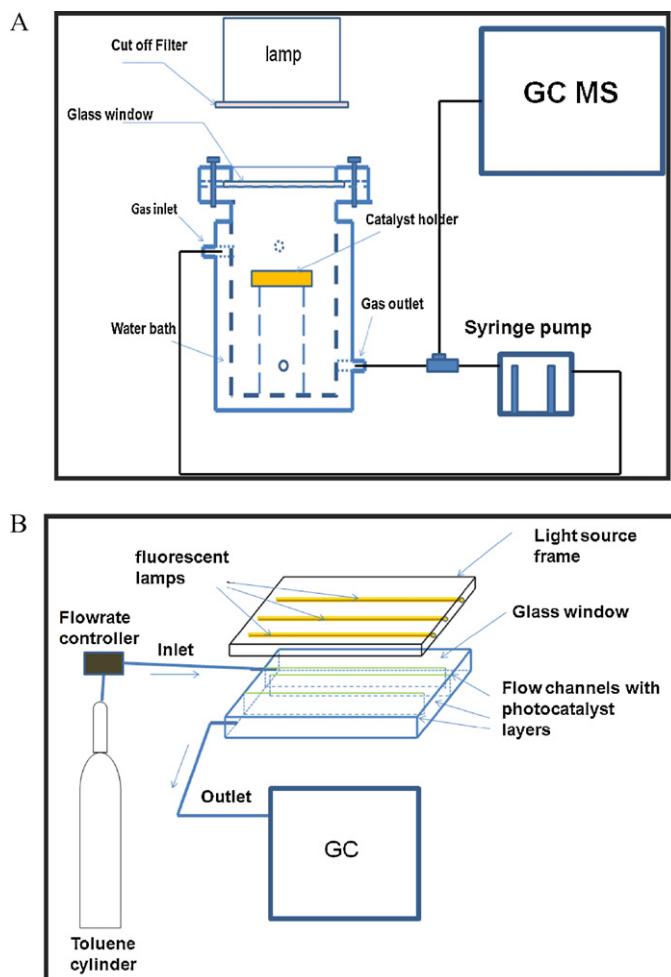


Fig. 1. Schematic diagrams of a batch reactor (A) and a continuous reactor (B) for degradation of VOCs.

the presence of NO_x , which can possibly be NO , NO_2 , NO_2^- and NO_2^{2-} , etc. The overall nitrogen doping level was estimated to be 0.75 at.% in this investigation. Fig. 2(B) shows XPS spectrum of Pt 4f_{7/2} and 4f_{5/2} energy regions on Pt/N-TiO₂. The integrated fitting peaks were at 72.3 and 75.7 eV, respectively, and the spin energy separation was 3.4 eV. The value was slightly higher than the characteristic value of metallic Pt (3.35 eV), indicating that the platinum species existing in the sample was dominated as Pt²⁺ with little amount of metallic Pt⁰ [24,25]. Iliev et al. [26] prepared a TiO₂ modified with platinum by a photoreduction method, the peak of Pt 4f_{7/2} was at 71 eV, suggesting the presence of Pt⁰. Kozlova et al. [27] reported that the chemical state of Pt varied with the preparation method. The peak at 72.4 eV of Pt 4f_{7/2}, arising from Pt²⁺ was observed even in the sample via the photoreduction process. In this study, the platinum was incorporated by a sol-gel process. The lower pH value in preparation and the presence of anionic species, such as NO_2^- and NO_2^{2-} would lead to the formation of Pt²⁺. The sample was annealed at 400 °C, Pt²⁺ could also be PtO or PtCl₂. Considering the complicated Pt XPS spectrum, the Pt-related groups were tentatively described as [PtNO_x·PtO_y·PtCl_z].

3.2. UV-vis diffuse reflectance spectra

For utilisation of room lights, which emit energies mainly in the region of 400 to 650 nm, the optical property of a photocatalyst is of critical importance. Fig. 3 displays DRS of Degussa P25 and Pt/N-TiO₂ photocatalysts. It was observed that the absorption

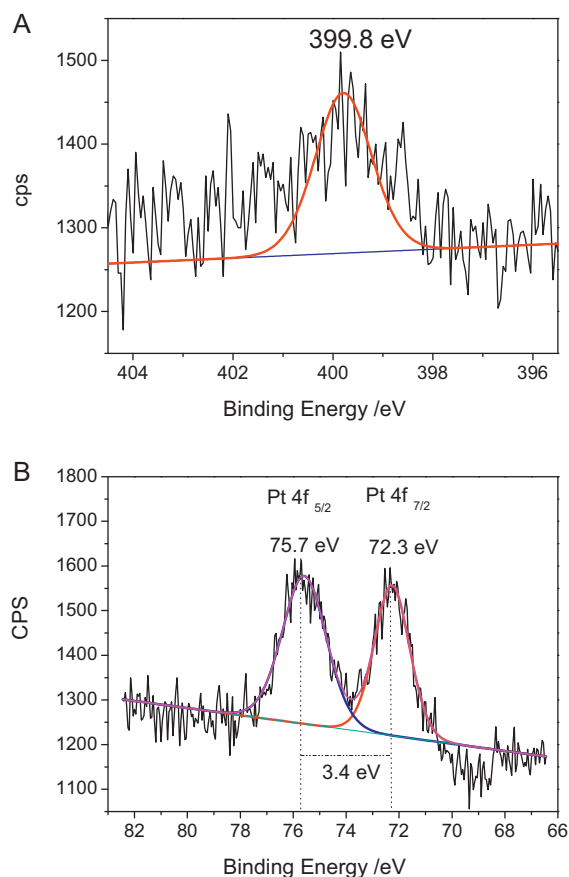


Fig. 2. N (1s) and Pt (4f) XPS spectra of Pt/N-TiO₂.

threshold of P25 was 400 nm with no absorption in visible light region (400–750 nm). The threshold of Pt/N-TiO₂ photocatalyst was successfully extended to ca. 495 nm, moreover, the absorption shoulder was observed in the whole visible region, further into infrared wavelength (IR). The band gap energies were estimated by the Kubelka–Munk equation, $(\alpha h\nu)^n = B(h\nu - E_g)$. In this study, $(\alpha h\nu)^n$ ($n=0.5$) versus $h\nu$ extrapolated to $\alpha=0$ represents the absorption band gap energy. The band gap of P25 was 3.10 eV, which was well in accordance with the results in literature [28]. The band gap energy was significantly narrowed to 2.69 eV by the modification of nitrogen and platinum. In the previous studies [13–15], nitrogen doping via wet-chemistry only slightly decreased the band gap of TiO₂. The greater band gap narrowing in this study was

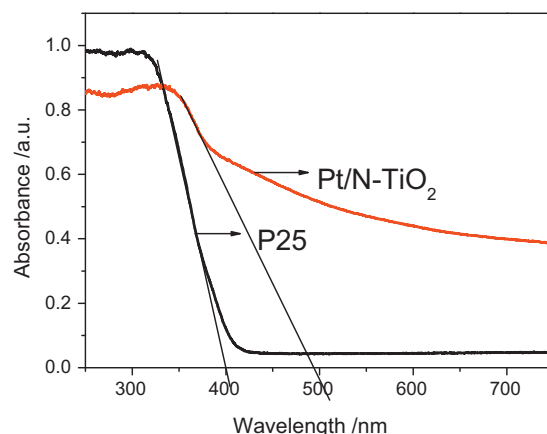


Fig. 3. UV-vis diffuse reflectance absorption spectra of P25 and Pt/N-TiO₂.

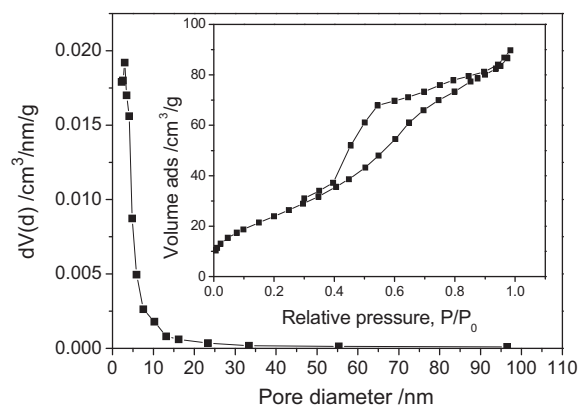


Fig. 4. Nitrogen adsorption-desorption isotherms and pore size distribution calculated from the desorption branch of the nitrogen isotherm by the BJH method.

possibly attributed to the co-presence of Pt^{2+} and N. Higashimoto et al. [29] reported that the HOMO-LUMO gap of the aqueous solutions of H_2PtCl_6 or PtCl_4 was estimated to be $E_g = 2.3\text{--}2.4$ eV. They used Pt salts to modify the surface of N-TiO₂ to obtain $\text{PtCl}_x/\text{N-TiO}_2$, achieving an absorption band around 2.3–2.4 eV. But the visible light absorption ended before 550 nm. Kowalska et al. [30] reported a DRS of Pt^{2+} modified TiO₂, which was similar to the result of this study.

3.3. Nitrogen isotherm

Fig. 4 shows nitrogen adsorption-desorption isotherms and pore size distribution of Pt/N-TiO₂. An IV-type N₂ isotherm with hysteresis loops indicated that the as-prepared photocatalyst was of mesoporous nature. There was a diffusion bottleneck, which was possibly from the nonuniform pore size [31]. An obvious hysteresis loop located at the high relative pressure region, which might show that the capillary condensation was associated with large pore channels [32]. The specific surface area of Pt/N-TiO₂ calculated from the BET plot was 94.5 m²/g. The BET surface area of P25 was 47.0 m²/g, same as the result reported before [30]. The pore size distribution calculated from the desorption branch of the nitrogen isotherm showed a narrow range of 3–8 nm. From the XRD profile (not shown here), the crystalline particle size of Pt/N-TiO₂ was only about 5 nm. The pores were possibly from the aggregation of the fine nano particles. The larger specific surface area and pore structure would be beneficial to attract the gaseous molecules onto the surface of the catalyst for fast degradation.

3.4. SEM image Pt/N-TiO₂ photocatalyst

Fig. 5 shows the SEM image of Pt/N-TiO₂. One can see that the material aggregated at some level, but also had many discrete particles. The size of discrete particles was about 10 nm, which was very close to the crystalline size of 5 nm from XRD profile. Iliev et al. [26] and Kozlova et al. [27] had applied Degussa P25 (20 nm, BET = 50 m²/g) as a supporting material for deposition of Pt, leading to a Pt particle with a size of 3–8 nm. In our study, both the particle size (ca. 10 nm) and BET (94.5 m²/g) were better than P25, expecting much smaller Pt size. From SEM image, it can be seen that the size of the aggregation was about hundreds of nanometres. As shown in N₂ isotherm, mesoporous structure was then produced.

3.5. Photocatalytic activity at varying wavelengths of light

Fig. 6 shows the photocatalytic performances of Pt/N-TiO₂ in photodegradation of phenol solutions under various irradiations.

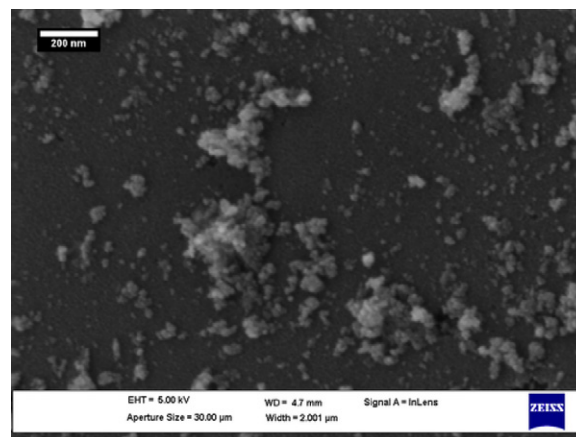


Fig. 5. SEM image of Pt/N-TiO₂ photocatalyst.

Under the irradiations with the wavelengths longer than 387 nm, P25 only degraded 63.9% of phenol in 120 min, meanwhile Pt/N-TiO₂ managed to completely destruct phenol in 60 min. Under $\lambda > 430$ nm, the reaction time was prolonged to 240 min for complete decomposition of phenol. At $\lambda > 490$ nm, 64% of phenol was photodegraded in 360 min. The results proved that Pt/N-TiO₂ was of higher visible light photocatalytic activity, complying with the DRS results. Based on the Langmuir-Hinshelwood mechanism [15], the apparent reaction rates of P25 and Pt/N-TiO₂ were 0.00934 and 0.0513 min⁻¹, respectively. The efficiency of Pt/N-TiO₂ was 5.5 times higher than the reference of P25. In our unpublished data, the apparent reaction rate of Pt (1.0 at. %)/TiO₂ was 0.0222 min⁻¹, 2.4 times higher than P25. Therefore, the synergistic effect between platinum and nitrogen was clearly demonstrated. The enhanced activity from Pt⁰ deposition has been widely known, as the Pt nanoparticles deposited on TiO₂ surface would capture the electrons, leading to a higher separation rate of photoinduced carriers [33]. Higashimoto et al. [34] reported that $\text{PtCl}_x/\text{N-TiO}_2$ had a much higher activity than Pt⁰/N-TiO₂ and they proposed a Z-scheme mechanism for charge separation between platinum chloride and N-TiO₂. In their studies, the $\text{PtCl}_x/\text{N-TiO}_2$ was prepared by a post-treatment of N-TiO₂ using platinum salts without calcination. In our studies, the sample can be more likely described as $\text{Pt}^{2+}(\text{NO}_x^{2-})\text{-TiO}_2$, which could contribute to the charge balance of the TiO₂ surface [23], leading to the higher activity. Both Pt^{2+} and NO_x^{2-} would act as the centers for absorption of visible light.

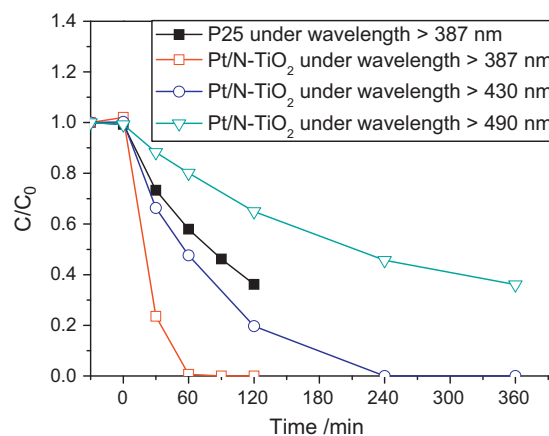


Fig. 6. Photodegradation of phenol solutions using P25 and Pt/N-TiO₂ under different irradiations. The lamp was switched on after 30 min of adsorption equilibrium [catalyst: 1 g/L, temperature: 30 °C, phenol initial concentration: 25 ppm].

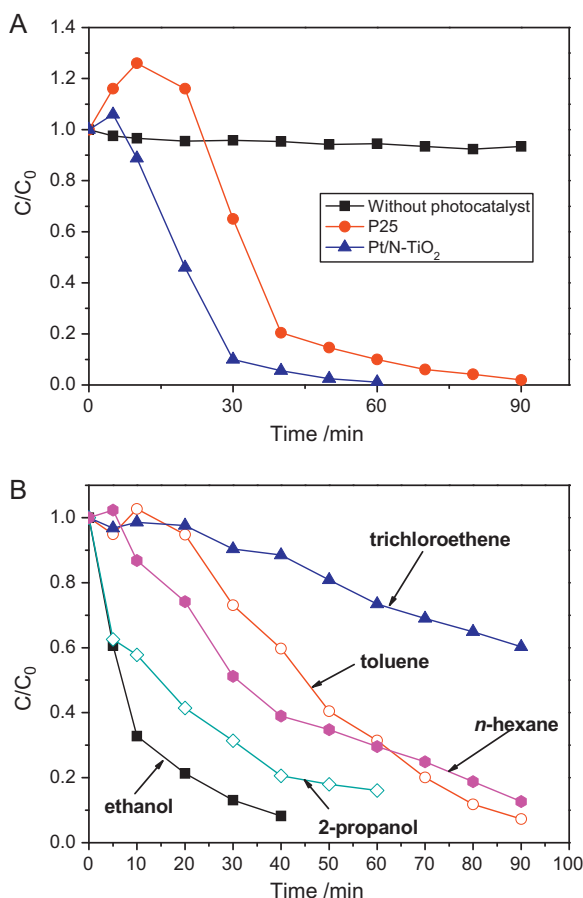


Fig. 7. Photocatalytic degradation of various gaseous compounds under UV-vis light. (A) Degradation of acetone using different photocatalysts and (B) Degradation of various chemicals using Pt/N-TiO₂ photocatalyst [temperature: 30 °C, light source: $\lambda > 386$ nm, initial concentration: ca. 200 ppm].

3.6. Photodegradation of various gaseous pollutants in a batch reactor ($\lambda > 387$ nm)

Fig. 7(A) shows the degradation of gaseous acetone under UV-vis light. In the control experiment, the concentration of acetone was stable without the photocatalyst, indicating the reliability of the experimental condition. In 90 min, acetone was completely degraded by P25. Pt/N-TiO₂ showed a superior activity to P25 and acetone was completely decomposed in 60 min. The increased activity of Pt/N-TiO₂ was consistent with the photodegradation of aqueous phenol (Fig. 6). Fig. 7(B) displays the performance of Pt/N-TiO₂ in the degradation of various gaseous pollutants, such as ethanol, 2-propanol, *n*-hexane, toluene, and TCE. It was observed that Pt/N-TiO₂ was capable in photodegradation of most above chemicals, varying efficiencies dependent on the nature of the substrates. Kim and Hong [35] examined the kinetics of photocatalytic degradation of VOCs including TCE, acetone, methanol and toluene, using TiO₂ thin film under UV. The photocatalytic conversion rates were in the order of TCE > methanol > acetone > toluene. Alberici and Jardim [6] compared the continuous degradation of various VOCs using TiO₂ under UV and the order of selected conversion rates were TCE > acetone > toluene > 2-propanol. It was deduced that the photocatalytic activity in degradation of VOCs varies greatly on the photocatalysts and experimental parameters.

In this study, a different order of conversion rates was observed. Generally for a photocatalyst, the performance in degradation would be controlled thermodynamically and kinetically by the reaction system. The efficiency would depend on, in terms of

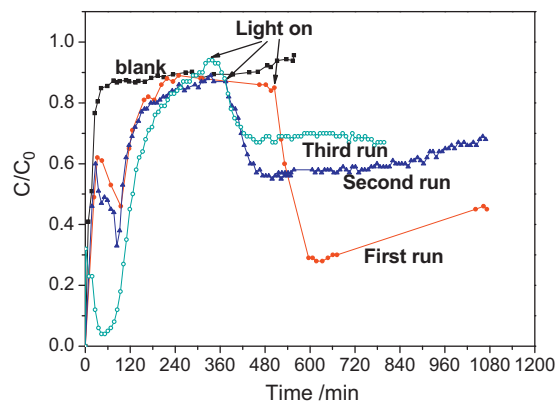


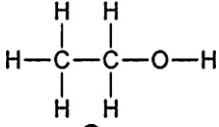
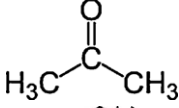
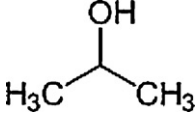
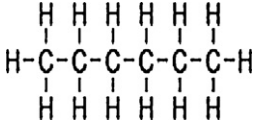
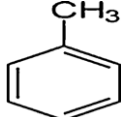
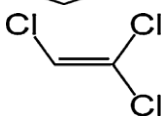
Fig. 8. Continuous photodegradation of 100 ppm toluene using Pt/N-TiO₂ [ambient temperature, atmospheric pressure, room lights].

substrates, the length and type of carbon chain, and binding energy. It would be also determined by the adsorption/desorption process, as well as temperature, pressure, oxygen content, and humidity, etc. Table 1 lists the chemicals, molecular weight, molecular structure, theoretical electrons consumption, and reaction rates of various VOCs. Except for TCE, there was a clear tendency that the conversion rates decreased at increased molecular weight and electron consumption. For C–H (or O-containing) compounds, molecular weight may reflect the electron consumption. The photoinduced carriers would be constant in an identical reaction condition over the same photocatalyst, thus the higher electron consumption, the lower conversion. Theoretically TCE would obtain the highest reaction rate, as shown by Alberici and Jardim [6] and Kim and Hong [35], however, such results were not proven by this study. The reduced TCE degradation would be possibly attributed to the changes in the surface feature of the catalyst, which controls the adsorption of substrates. For Pt/N-TiO₂, its surface was changed to be acidic by the acid-catalysed sol-gel and the presence of Pt species. Thus different from pristine TiO₂ surface, the modified surface would no longer favour the degradation of TCE, which might produce HCl during the oxidation on the surface as well. The chemical structure was not found to play a key role in the performance of Pt/N-TiO₂ in degradation of VOCs.

3.7. Room light induced degradation of gaseous toluene at continuous phase

Fig. 8 shows the photodegradation of gaseous toluene at continuous flow. The experimental condition was set at ambient temperature, atmospheric pressure, and room lights. In a blank test, the concentration from outlet of the reactor reached quasi-stable phase in 60 min, indicating the complete flush of the air in the reactor. The concentration would be then increased very slowly to reach initial concentration of toluene. Once the photocatalyst was loaded into the reactor, the flushing process was repeated. Due to the purging process and adsorption on the photocatalyst, the toluene concentration fluctuated in the first 5 h. This might suggest the adsorption of gaseous toluene on photocatalyst layer due to large BET surface area, as shown in N₂ isotherm. Once the concentration became stable, the fluorescent lamps (6 × 10 W) were switched on. The concentration of toluene was observed to decrease rapidly, and reached a stable stage in 90 min. In the first run, the highest degradation rate of toluene was 70%. Due to the incomplete decomposition, the intermediates or coke would deactivate the photocatalyst. The degradation rate of toluene decreased to be 55% after 500 min reaction. The stability of Pt/N-TiO₂ was further tested by the second and third runs. No regeneration process

Table 1
Molecular weight, molecular structure, minimum electrons consumption, and apparent rate constant of various VOCs.

Chemicals	Molecular weight	Molecular structure	Minimum electrons consumption ^a (mol/mol)	Apparent rate constant ^b /min ⁻¹	Regression coefficient (R^2)
Ethanol	46.07		12	0.0920	0.973
Acetone	58.08		16	0.0437	0.881
2-Propanol	60.10		17	0.0430	0.912
<i>n</i> -Hexane	86.18		34	0.0204	0.974
Toluene	92.14		36	0.0170	0.878
Trichloroethene	131.4		4	0.0049	0.930

^a Electrons consumption was deduced from the stoichiometric ratio of oxygen involved, molar electrons vs. molar VOC.

^b For simple comparison, a pseudo first order kinetics was applied for fitting.

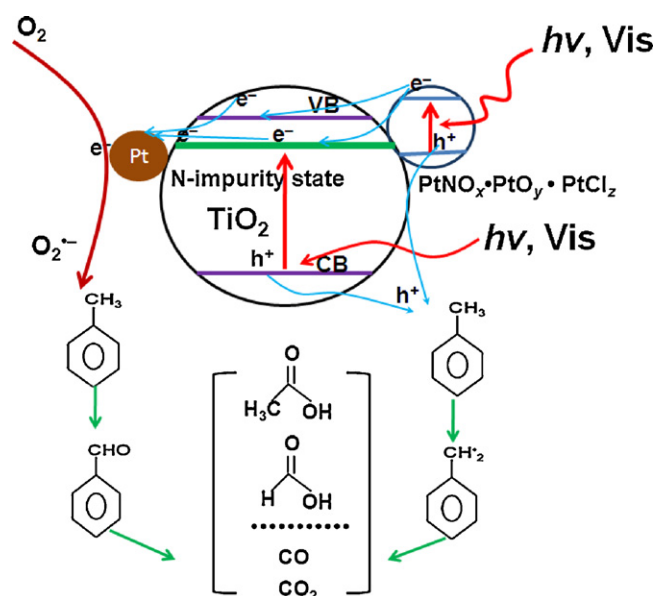
was taken, but the reactor was flushed by air thoroughly before each run. In the second run the toluene conversion decreased to 45%, and 31% in the third run.

In photocatalytic degradation of gaseous toluene, a range of by-products would be produced, such as formaldehyde, methanol, propylene, acetic acid, benzene, benzoic acid, etc. [36] The deactivation of a photocatalyst was very common in UV photocatalysis [37] and becomes worse under visible light. In this study, the applied light sources were pale room lights, thus the obtained stability was very promising and competitive. It is expected that, the performance in decomposition of lower level VOCs, i.e. indoor air level, will be much close to feasible application.

3.8. Mechanism of photodegradation of gaseous toluene over Pt/N-TiO₂ under room lights

Scheme 1 shows a tentative mechanism to illustrate the processes of light activation, charge transfer and photooxidation of gaseous toluene under visible light. N doping might create impurity states under the bottom of conduction band of TiO₂, making TiO₂ be activated by visible light [15,38]. The Pt species, previously described as [PtNO_x·PtO_y·PtCl_z], would be also activated by visible light and inject the photoinduced electrons to the conduction band and impurity band of TiO₂ [29,39]. The presence of little amount Pt⁰ would trap the electrons and increase the separation of photoinduced electron/hole pairs. The produced holes (h⁺) would migrate to the surface of the photocatalyst for direct oxidation, though part of them would be quenched by electrons and released as heat in the bulk or on the surface. The photooxidation pathways of gaseous toluene were suggested as OH[•], O₂^{•-}, and h⁺ oxidations [40,41]. In the present study, water vapour was minimised by using

cylinder gas through an air-free reactor. Thus, except for minor surface hydroxyl radicals, O₂^{•-} and h⁺ would mainly contribute to the oxidation via different intermediates, the both oxidants would lead to the ring opening of toluene, eventually oxidise it to CO₂. Meanwhile, the intermediates that did not undergo complete oxidation might result in the deactivation of the photocatalyst.



Scheme 1. Mechanism of photodegradation of gaseous toluene over Pt/N-TiO₂ under visible light irradiations.

4. Conclusions

In conclusion, a highly efficient visible light photocatalyst of Pt/N-TiO₂ was prepared by a modified sol–gel process. The photocatalyst showed 5.5 times higher activity than P25 and could efficiently photodegrade aqueous phenol even under $\lambda > 490$ nm. Various VOCs, such as ethanol, acetone, 2-propanol, *n*-hexane, toluene and TCE, were able to be decomposed. Continuous tests further proved that gaseous toluene (100 ppm) was able to be degraded under room lights. This study underpins a potential design of a conceptual air purifier by utilisation of spare room lights.

References

- [1] S.B. Wang, H.M. Ang, M.O. Tade, *Environ. Int.* 33 (2007) 694–705.
- [2] S.H. Chong, S.B. Wang, M. Tade, H.M. Ang, V. Pareek, *AIChE J.* 57 (2011) 724–734.
- [3] F. Thevenet, O. Guaitella, E. Puzenat, J.M. Herrmann, A. Rousseau, C. Guillard, *Catal. Today* 122 (2007) 186–194.
- [4] F.Y. Yi, X.D. Lin, S.X. Chen, X.Q. Wei, J. Porous Mater. 16 (2009) 521–526.
- [5] K. Everaert, J. Baeyens, J. Hazard. Mater. 109 (2004) 113–139.
- [6] R.M. Alberici, W.E. Jardim, *Appl. Catal. B: Environ.* 14 (1997) 55–68.
- [7] I. Salvado-Estivill, D. Hargreaves, G. Puma, *Environ. Sci. Technol.* 41 (2007) 2028–2035.
- [8] J. Jeong, K. Sekiguchi, K. Sakamoto, *Chemosphere* 57 (2004) 663–671.
- [9] D. Kibanova, J. Cervini-Silva, H. Destailats, *Environ. Sci. Technol.* 43 (2009) 1500–1506.
- [10] X.G. Qu, W.X. Liu, J. Ma, W.B. Cao, *Res. Chem. Intermed.* 35 (2009) 313–320.
- [11] A.V. Vorontsov, E.N. Kurkin, E.N. Savinov, *J. Catal.* 186 (1999) 318–324.
- [12] A.L. Linsebigler, G.Q. Lu, J.T. Yates, *Chem. Rev.* 95 (1995) 735–758.
- [13] H.Q. Sun, Y. Bai, W.Q. Jin, N.P. Xu, *Solar Energy Mater. Solar Cells* 92 (2008) 76–83.
- [14] H.Q. Sun, Y. Bai, H.J. Liu, W.Q. Jin, N.P. Xu, G.J. Chen, B.Q. Xu, *J. Phys. Chem. C* 112 (2008) 13304–13309.
- [15] H.Q. Sun, Y. Bai, H.J. Liu, W.Q. Jin, N.P. Xu, *J. Photochem. Photobiol. A: Chem.* 201 (2009) 15–22.
- [16] W.K. Jo, J.T. Kim, *J. Hazard. Mater.* 164 (2009) 360–366.
- [17] S. Higashimoto, Y. Ushiroda, M. Azuma, *J. Nanosci. Nanotechnol.* 10 (2010) 246–251.
- [18] X. Zhang, Q.Q. Liu, *Appl. Surf. Sci.* 254 (2008) 4780–4785.
- [19] L.H. Huang, C. Sun, Y.L. Liu, *Appl. Surf. Sci.* 253 (2007) 7029–7035.
- [20] X. Yang, Y.H. Wang, L.L. Xu, X.D. Yu, Y.H. Guo, *J. Phys. Chem. C* 112 (2008) 11481–11489.
- [21] P.G. Wu, R.C. Xie, K. Imlay, J.K. Shang, *Environ. Sci. Technol.* 44 (2010) 6992–6997.
- [22] D.Z. Li, Z.X. Chen, Y.L. Chen, W.J. Li, H.J. Huang, Y.H. He, X.Z. Fu, *Environ. Sci. Technol.* 42 (2008) 2130–2135.
- [23] H. Sun, Y. Bai, Y. Cheng, W. Jin, N. Xu, *Ind. Eng. Chem. Res.* 45 (2006) 4971–4976.
- [24] M. Zhang, Z.S. Jin, J.W. Zhang, Z.J. Zhang, H.X. Dang, *J. Mol. Catal. A: Chem.* 225 (2005) 59–63.
- [25] M.A. Aramendia, J.C. Colmenares, A. Marinas, J.M. Marinas, J.M. Moreno, J.A. Navio, F.J. Urbano, *Catal. Today* 128 (2007) 235–244.
- [26] V. Iliev, D. Tomova, L. Bilyarska, A. Eliyas, L. Petrov, *Appl. Catal. B: Environ.* 63 (2006) 266–271.
- [27] E.A. Kozlova, T.P. Lyubina, M.A. Nasalevich, A.V. Vorontsov, A.V. Miller, V.V. Kaichev, V.N. Parmon, *Catal. Commun.* 12 (2011) 597–601.
- [28] J.A. Rengifo-Herrera, J. Kiwi, C. Pulgarin, *J. Photochem. Photobiol. A: Chem.* 205 (2009) 109–115.
- [29] S. Higashimoto, K. Takamatsu, M. Azuma, M. Kitano, M. Matsuoka, M. Anpo, *Catal. Lett.* 122 (2008) 33–36.
- [30] E. Kowalska, H. Remita, C. Colbeau-Justin, J. Hupka, J. Belloni, *J. Phys. Chem. C* 112 (2008) 1124–1131.
- [31] J.C. Yu, J.G. Yu, W.K. Ho, Z.T. Jiang, L.Z. Zhang, *Chem. Mater.* 14 (2002) 3808–3816.
- [32] T.Y. Peng, H.B. Song, H.R. Xiao, H.J. Liu, J. Qin, *J. Non-Cryst. Solids* 352 (2006) 3167–3174.
- [33] B. Sun, A.V. Vorontsov, P.G. Smirnotis, *Langmuir* 19 (2003) 3151–3156.
- [34] S. Higashimoto, Y. Ushiroda, M. Azuma, H. Ohue, *Catal. Today* 132 (2008) 165–169.
- [35] S.B. Kim, S.C. Hong, *Appl. Catal. B: Environ.* 35 (2002) 305–315.
- [36] J.H. Mo, Y.P. Zhang, Q.J. Xu, Y.F. Zhu, J.J. Lamson, R.Y. Zhao, *Appl. Catal. B: Environ.* 89 (2009) 570–576.
- [37] C. Akly, P.A. Chadik, D.W. Mazyck, *Appl. Catal. B: Environ.* 99 (2010) 329–335.
- [38] T. Lindgren, J.M. Mwabora, E. Avendano, J. Jonsson, A. Hoel, C.G. Granqvist, S.E. Lindqvist, *J. Phys. Chem. B* 107 (2003) 5709–5716.
- [39] F. Dong, H.Q. Wang, G. Sen, Z.B. Wu, S.C. Lee, *J. Hazard. Mater.* 187 (2011) 509–516.
- [40] M. Sleiman, P. Conchon, C. Ferronato, J.M. Chovelon, *Appl. Catal. B: Environ.* 86 (2009) 159–165.
- [41] H.B. Huang, W.B. Li, *Appl. Catal. B: Environ.* 102 (2011) 449–453.